# Open Research Online

# The European Large Area *ISO* Survey – III.
# 90-μm extragalactic source counts

Andreas Efstathiou,[1]★ Seb Oliver,[1,2] Michael Rowan-Robinson,[1] C. Surace,[1] T. Sumner,[1]
P. Héraudeau,[3] M. J. D. Linden-Vørnle,[4] D. Rigopoulou,[5] S. Serjeant,[1] R. G. Mann,[1]
C. J. Cesarsky,[6] L. Danese,[7] A. Franceschini,[8] R. Genzel,[5] A. Lawrence,[9] D. Lemke,[3]
R. G. McMahon,[10] G. Miley,[11] J.-L. Puget[12] and B. Rocca-Volmerange[13]

[1]*Astrophysics Group, Blackett Laboratory, Imperial College of Science Technology & Medicine, Prince Consort Road, London SW7 2BZ*
[2]*Astronomy Centre, University of Sussex, Falmer, Brighton BN1 9QJ*
[3]*Max-Planck-Institut für Astronomie, Königstuhl 17, D-69117, Heidelberg, Germany*
[4]*Danish Space Research Institute, Juliane Maries Vej 30, DK-2100 Copenhagen Ø, Denmark*
[5]*Max-Planck-Institut für extraterrestrische Physik, Postfach 1603, 85740 Garching, Germany*
[6]*CEA/SACLAY, 91191 Gif sur Yvette cedex, France*
[7]*SISSA, International School for Advanced Studies, Via Beirut 2-4, 34014 Trieste, Italy*
[8]*Dipartimento di Astronomia, Università di Padova, Vicolo Osservatorio 5, I-35122 Padova, Italy*
[9]*Institute for Astronomy, University of Edinburgh, Royal Observatory, Blackford Hill, Edinburgh EH9 3HJ*
[10]*Institute of Astronomy, The Observatories, Madingley Road, Cambridge CB3 0HA*
[11]*Leiden Observatory, PO Box 9513, NL-2300 RA Leiden, the Netherlands*
[12]*Institut d'Astrophysique Spatiale, Bâtiment 121, Université Paris XI, 91405 Orsay cedex, France*
[13]*Institut d'Astrophysique de Paris, 98bis Boulevard Arago, F 75014 Paris, France*

**ABSTRACT**

We present results and source counts at 90 μm extracted from the preliminary analysis of the
European Large Area *ISO* Survey (ELAIS). The survey covered about 12 deg² of the sky in
four main areas and was carried out with the ISOPHOT instrument onboard the *Infrared
Space Observatory* (*ISO*). The survey is at least an order of magnitude deeper than the *IRAS*
100-μm survey and is expected to provide constraints on the formation and evolution of
galaxies. The majority of the detected sources are associated with galaxies on optical
images. In some cases the optical associations are interacting pairs or small groups of
galaxies, suggesting that the sample may include a significant fraction of luminous infrared
galaxies. The source counts extracted from a reliable subset of the detected sources are in
agreement with strongly evolving models of the starburst galaxy population.

**Key words:** surveys – galaxies: evolution – galaxies: formation – galaxies: Seyfert –
galaxies: starburst – infrared: galaxies.

## 1 INTRODUCTION

As is well known, a large fraction of the bolometric luminosity of
galaxies is emitted at far-infrared wavelengths as a result of
reprocessing of starlight by dust. The spectra of galaxies observed
by *IRAS* typically peak in the 60–100 μm range. Observations of
galaxies in the far-infrared are therefore essential for determining
the star formation rate and dust masses of galaxies. Interest in
dust-enshrouded galaxies has recently been renewed by the
discovery of a far-infrared (140–850 μm) background, thought
to be caused by discrete sources (Puget et al. 1996; Fixsen et al.
1998; Hauser et al. 1998; Lagache et al. 1998), and detections of

high-redshift galaxies with SCUBA (Smail et al. 1997; Barger
et al. 1998; Hughes et al. 1998; Eales et al. 1999), which are
thought to be primeval analogues of the starburst galaxies
observed locally. Deep surveys in the far-infrared therefore
promise to be very useful for understanding galaxy formation
and evolution, as they can recover information missed by optical/
ultraviolet studies (e.g. Madau et al. 1996; Steidel et al. 1996).
Studies of infrared galaxies detected by *IRAS* suggest that violent
episodes of star formation are usually associated with very high
dust optical depths (Condon et al. 1991; Rowan-Robinson &
Efstathiou 1993; Franceschini et al. 1994), which usually exceed
unity even at 60 μm. Models of dusty tori in active galactic nuclei
(AGN; Pier & Krolik 1992; Granato & Danese 1994; Efstathiou &
Rowan-Robinson 1995) also suggest that the optical depths of

★ E-mail: a.efstathiou@ic.ac.uk

type 2 objects are at least as high. Observations of galaxies with *ISO* seem to have detected colder dust than observed by *IRAS* (Bogun et al. 1996; Krügel et al. 1998).

The European Large Area *ISO* Survey [ELAIS; for a thorough description of the survey and its goals see Oliver et al. (2000), Paper I], which surveyed about 12 deg² of the sky at 15 and 90 μm (and smaller areas at 6.7 and 175 μm) in mainly four (low-cirrus) areas spread over the northern and southern sky, and other *ISO* surveys (Kawara et al. 1998; Dole et al. 1999; Puget et al. 1999) represent the first opportunity since *IRAS* to study the properties and evolution of the far-infrared galaxy populations at intermediate redshift. An extensive follow-up programme from radio to X-ray wavelengths, already under way, ensures that the ELAIS detected galaxies will be the subject of thorough study for the next few years.

In this paper we describe the pipeline developed for the production of the ELAIS preliminary analysis (EPA) 90-μm catalogue and present source counts. A previous paper by Serjeant et al. (2000, Paper II) presented the 6.7- and 15-μm pipeline and counts. Oliver et al. (in preparation) present an analysis of the multiply covered ELAIS areas. Serjeant et al. present the preliminary 90-μm luminosity function.

The paper is organized as follows. In Section 2 we describe the data reduction and source extraction methods used. In Section 3 we discuss tests for assessing the reliability and completeness of

the survey including comparisons with a parallel pipeline to be described in a separate paper (Surace et al., in preparation). In Section 4 we present the source counts. In Section 5 we discuss briefly our results and outline our conclusions.

## 2   OBSERVATIONS AND REDUCTION

As described in detail in Paper I, the data consists of a number of pointed observations (in raster mode) which use the $3 \times 3$ array of the ISOPHOT instrument (Lemke et al. 1996) onboard *ISO* (Kessler et al. 1996). The area covered by each raster was typically about 0.25 deg². The integration time at each raster position varied but it was typically 20 s. The initial observing mode did not allow for any redundancy. Analysis of some of the early rasters indicated that the efficiency and reliability of the survey could be significantly improved with some redundancy, so for the latter half or so of the survey we switched to an 'overlapping mode' so that each part of the sky observed thereafter was covered at least twice. Some areas of the survey were observed on more than one occasion, thus providing further redundancy and depth.

The survey was carried out in four main areas (three in the northern and one in the southern hemisphere) and some smaller areas of special scientific interest (Paper I).

The pipeline we developed for the preliminary analysis consists of two basic stages. In the first stage we process the raw data using
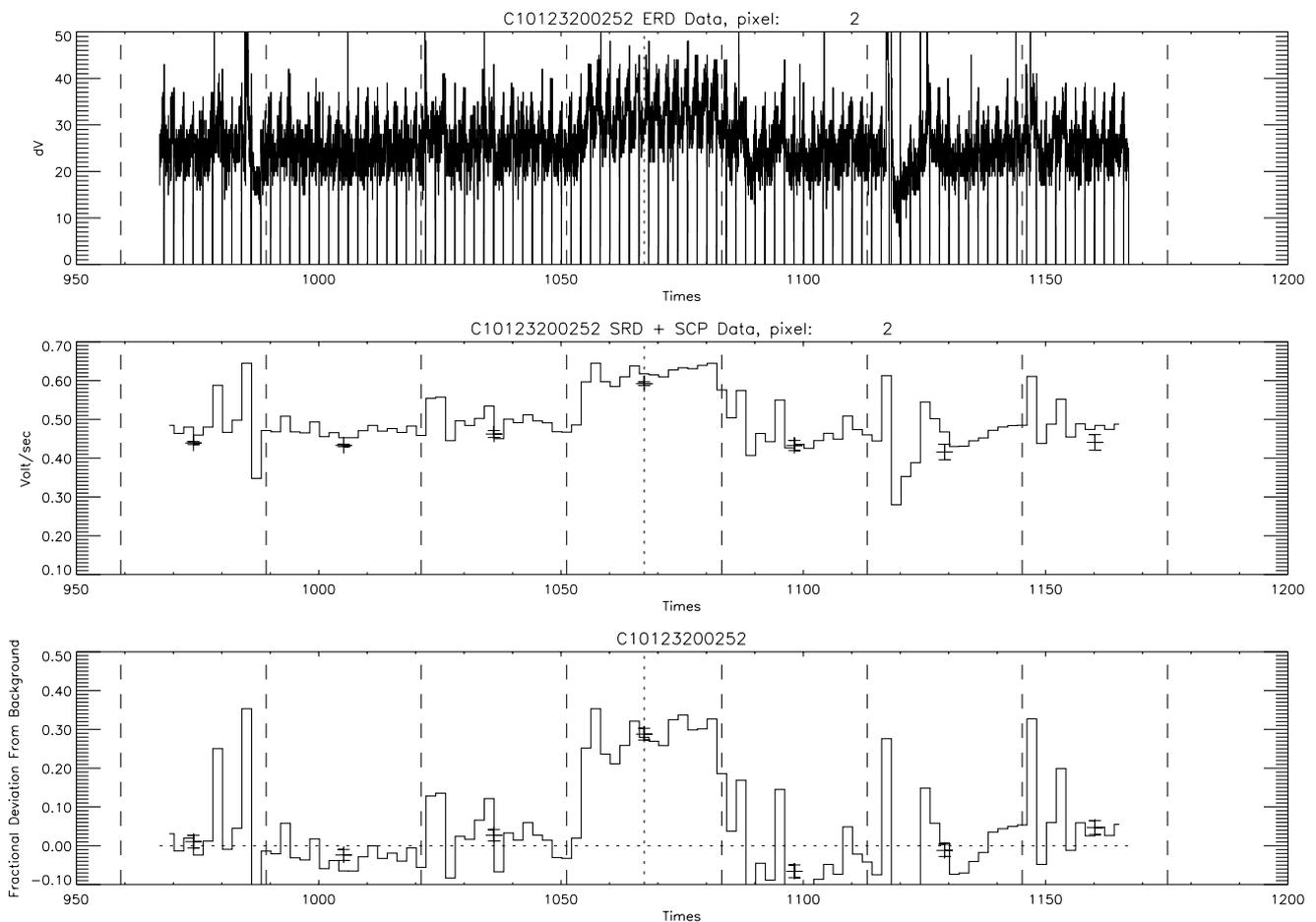


**Figure 1.** Timeline of a typical source with *qual* = 1 (definite detection). The top panel shows the raw data (in the form of the difference d*V* between successive readouts in volts) for about 100 s centred on the expected time of pointing at the source (dotted vertical line). The dashed vertical lines show the time the telescope starts slewing on to a new position. The middle panel shows the data at the end of the PIA stage of the data reduction. The bottom panel shows the fractional deviation from the background after the median filtering.

the standard PHOT interactive analysis (PIA) software (Gabriel et al. 1997) until we derive a signal per 2-s integration ramp. This involves discarding some readouts at the beginning of the ramp, and treatment of cosmic rays. The data stream includes data recorded while the telescope is slewing between pointings (this typically takes 2 or 3 s per pointing).

The second stage of our analysis, performed with purpose-built IDL (Interactive Data Language) routines, involves the extraction of point sources from the timeline of each of the nine pixels of the PHOT array. Given the poor understanding of the instrument flat-field at the time it was considered premature to try to extract sources from maps. Our source extraction method is therefore very different from that employed in deep 175-μm surveys where multiple redundancy and detector stability allow more traditional and reliable techniques to be employed (Kawara et al. 1998; Dole et al. 1999; Puget et al. 1999). For each pixel we ran an iterative median filter that removed outliers (arising from cosmic rays) and determined the fractional deviation from the background, $\rho$, for each ramp. Pointings for which the weighted average of $\rho$ over the pointing, $\bar{\rho}$, exceeded a certain threshold ($3\sigma_{\bar{\rho}}$) were flagged as potential point sources.

The pipeline produced source lists on a raster-by-raster basis and typically yielded ~0.08 detections per pointing per pixel. Unfortunately, visual scanning of the time profiles of the potential sources revealed that only a small fraction of them are likely to be real sources. There are a number of effects that can give rise to spurious sources and some of these are illustrated in Fig. 1.

Fig. 1 shows the data stream of one pixel for about six pointings centred on a very clear detection of a source (at $t \approx 1050$–$1085$ s) at different stages of the processing. Note the delay in the signal response to the change in illumination (about 2–3 s), which is partly a result of the movement of the telescope into position and arises partly from the hysteresis of the detector. The latter is also responsible for the gradual fading of the signal at the end of the pointing. The occurrence of these effects at the beginning and end of the pointing leaves little doubt as to the reality of the detection.

The source profiles are usually more complicated than that shown in Fig. 1, owing to the occurrence of cosmic ray events. Examples of such events can be seen on the same stream of data. Note, for example, the dips in the signal after the spikes at $t \approx 985$ and 1115 s, and the fading profile after a spike at $t \approx 1125$ s. In addition, the C100 detectors sometimes display a drift behaviour which can give the appearance of a source if the peak of the cycle coincides with the centre of a pointing.

While a procedure for automatic filtering of false detections was developed it was found to be unreliable. The time profiles of all potential sources were therefore visually scanned by at least two observers in order to construct the final source list. Five different classifications (*qual*) were used ranging from 1 (definite detection; see Fig. 1) to 5 (severely affected by cosmic rays).

### 2.1 Flux calibration

The standard method of flux calibration of the PHOT instrument is to make use of the internal fine calibration source (FCS; Schulz et al. 1998). The FCS has been calibrated using planets and asteroids at bright fluxes and stars at faint fluxes. The FCS is observed immediately before and after each raster in order to monitor the change in the responsivity of the detector over the course of the raster. Despite the best efforts of the instrument team, the calibration obtained in this way was considered until recently to be of only qualitative value. It is now thought to be

uncertain by about 20–30 per cent depending on the type of observation. This motivated us to pursue an alternative method for the flux calibration for the EPA which makes use of celestial standards such as the 100-μm background measured by *COBE/IRAS* and *IRAS* sources. The application of a method based on celestial standards on a large and homogeneous data set such as ELAIS can also provide an independent check on the FCS method and provide insight into the characteristics of the instrument.

The basic steps followed in our method can be summarized as follows.

(i) Determine the flux per pixel $F_{\nu,\text{det}}$ (in Jy) of each detection by multiplying $\bar{\rho}$ by the predicted background flux incident on the pixel $F_\nu \equiv I_\nu\Omega$, where $I_\nu$ is the predicted background intensity and $\Omega$ is the solid angle ($0.44468 \times 10^{-7}$ sr; Klaas et al. 1994) subtended by a C100 ($43.5 \times 43.5$ arcsec$^2$) pixel.

(ii) Find an empirical conversion factor $f_{\text{p}\rightarrow\text{t}}$ for converting $F_{\nu,\text{det}}$ to a total flux for a point source centred on the pixel $F_{\nu,\text{src}}$. This factor is determined by comparing the corrected fluxes with those of calibration stars and *IRAS* sources and includes corrections for the point spread function (PSF), stray light, etc. We will find that $f_{\text{p}\rightarrow\text{t}}$ is the ratio of two factors $f_{\text{bckg}}$ and $f_{\text{psf}}$. The factor $f_{\text{bckg}}$ corrects our background estimate for the effective solid angle, stray light, etc. and $f_{\text{psf}}$ corrects for the fact that only a fraction of the flux from a point source will be recorded by a single-pixel detection.

The great advantage of the method is its transparency. Its validity ultimately depends on the accuracy with which the background can be estimated (given that it is dominated by the zodiacal emission which varies with the time of observation) and on the accuracy of the fluxes of the sources used as calibrators.

In the rest of this section we describe how we estimate the background, $f_{\text{bckg}}$ and $f_{\text{psf}}$, and test our calibration with stars and *IRAS* sources. Readers who are not interested in the details of these estimates and tests can find a summary of our results in Section 2.5.

### 2.2 Background estimate

Initially, we used the *COBE* background (obtained from the IRSKY service at IPAC) which gave us very poor spatial resolution. Our approach was subsequently refined to consider the separate contributions from the local (zodiacal) background, which depends on the time of observation, and Galactic and extragalactic components.

The background is estimated by combining the contributions of Galactic emission from the 100-μm maps of Schlegel, Finkbeiner & Davis (1998) and a model for the zodiacal light.

The zodiacal light emission depends on the ecliptic latitude $\beta$ and the solar elongation $e$ (e.g. CAM manual). It is worth noting that owing to observing constraints for the satellite, the solar elongation of most *ISO* observations was in the range 60°–120°. With the exception of two small areas (X3 and X6) $|\beta|$ for the ELAIS areas lies between 40° and 75°.

The zodiacal model used is based on the model described in the CAM manual (p. 77) which gives the zodiacal background at 10.9 μm as a function of $\beta$ and (more crudely) $e$. The predicted 10.9-μm background from this model is about 30 per cent higher than that measured by ISOCAM towards the ecliptic plane ($e = 104°$ and $\beta = -2°.4$; Reach et al. 1996) with the quoted uncertainty of ISOCAM calibration at the time being 15 per cent.

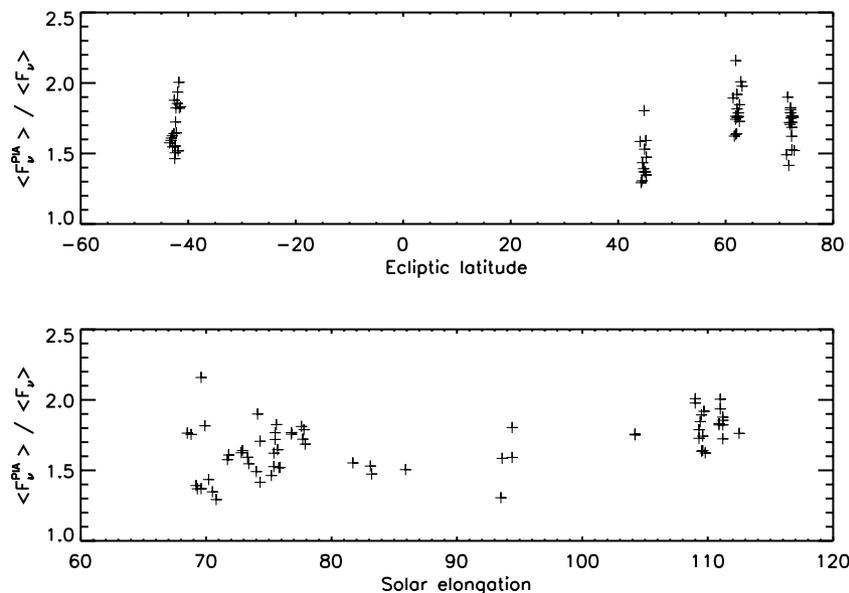To extrapolate to far-infrared wavelengths we assume that the

**Figure 2.** A plot of the ratio of the background obtained using PIA (averaged over all pointings/pixels in a raster) $\langle F_\nu^{\mathrm{PIA}}\rangle$ and that from our estimate from a model of the zodiacal background and maps of galactic emission $\langle F_\nu\rangle$ as a function of ecliptic latitude $\beta$ (top panel) and solar elongation (bottom panel).

spectrum of the zodiacal light can be modelled as a blackbody at a (constant) temperature of 275 K (Hauser et al. 1984). This model gives a ratio of $100\,\mu\mathrm{m}/25\,\mu\mathrm{m}$ backgrounds of 0.16, in very good agreement with the estimate of Schlegel et al. (1998).

In general, the temperature of the dust in the zodiacal cloud could vary with $\beta$ and $e$ (as our line of sight through the zodiacal cloud samples dust at varying distances from the Sun) but this is unlikely to affect the estimated background by more than 5–10 per cent (Schlegel et al.). The range of $|\beta|$ and $e$ spanned by the ELAIS survey observations is also quite narrow.

In Fig. 2 we compare our background estimate $F_\nu$, with the flux per pixel determined by PIA[1] using the FCS calibration, $F_\nu^{\mathrm{PIA}}$. We find that the ratio of the two raster-averaged estimates $f_{\mathrm{bckg}} = \langle F_\nu^{\mathrm{PIA}}\rangle/\langle F_\nu\rangle$ has a median value of 1.7. The origin of this difference is unclear but it may be related to the incidence of stray light on the detector. What is very encouraging is that if we multiply our estimate of the background by $f_{\mathrm{bckg}}$, it agrees with that determined by PIA to within 15 per cent.

### 2.3 ELAIS calibration stars

Given that there are no bright ($S > 0.6\,\mathrm{Jy}$) 12-$\mu$m sources in the ELAIS fields (to avoid saturating ISOCAM) we do not expect any 'photospheric' stars to be detected at $90\,\mu$m as these would have a 90-$\mu$m flux $\leqslant 10\,\mathrm{mJy}$. It is possible that there may be some stars with circumstellar dust shells, but the usefulness of such stars as calibrators would be limited. In order to better determine the ELAIS calibration (and the general ISOPHOT calibration) three stars (HR 6132, 6464 and 5981) close to the ELAIS fields were observed in mini-raster mode (a $3 \times 3$ raster with the star positioned at the centre of a different pixel in each pointing). These stars also formed part of the *ISO* ground-based preparatory programme. Models for their far-infrared (IR) spectra were constructed by fitting near-IR data and extrapolating to longer wavelengths as $\nu^2$ (Hammersley et al. 1998). A more empirical approach was given by Cohen et al. (1999). We use Hammersley's

[1] We refer here to the quantity phtiaap.mnfl produced by PIA Version 7.3.

predictions for the two brighter stars but for HR 5981 we use the prediction of Cohen as it is more reliable for cool stars. The predicted stellar fluxes (after convolving with the *ISO* 90-$\mu$m filter response) lie in the range 68–311 mJy, and so extend the flux range to fainter fluxes than is possible with the *IRAS* catalogued sources (see Section 2.4). The *IRAS* fluxes of these stars agree very well with the model up to $60\,\mu$m. At $100\,\mu$m results from SCANPI (also known as ADDSCAN) for the two brightest stars, which show significant detections, also show an excess over the models by factors of 2–5. It is not clear whether this implies that the stars have an infrared excess (e.g. caused by dust) or whether the SCANPI results suffer from some artefact introduced in the processing (e.g. by cirrus structure). The faintest of the stars (HR 5981) was observed twice on the same *ISO* orbit. The integration time per pointing in these mini-rasters (40 s) is longer than that used for the bulk of the ELAIS survey. The mini-rasters for the calibration stars were processed in the same way as the survey rasters.

In principle, each detection of each of the stars can be used to estimate $f_{\mathrm{p}\rightarrow\mathrm{t}}$, i.e. the correction factor for peak flux $F_{\nu,\mathrm{det}}$ to total flux $F_{\nu,\mathrm{src}}$ for our particular observing mode and in the ideal situation where a point source is centred in the pixel. We find the median value of $f_{\mathrm{p}\rightarrow\mathrm{t}}$ to be 2.8. In Fig. 3 we plot the ratio of $f_{\mathrm{p}\rightarrow\mathrm{t}}F_{\nu,\mathrm{det}}$ over the predicted stellar flux for each detection. As expected, the empirically estimated $f_{\mathrm{p}\rightarrow\mathrm{t}}$ is $\sim f_{\mathrm{bckg}}/f_{\mathrm{psf}}(0,0)$ where $f_{\mathrm{psf}}(0,0) = 0.6$ is the theoretically predicted fraction of total flux in the central pixel (Klaas et al. 1994; Laureijs 1999).

### 2.4 Comparison with *IRAS* sources

While the ELAIS fields were chosen to avoid strong infrared sources, there are a number of IRAS 100-$\mu$m sources in the PSC and FSC which were detected in the survey, some of them in a number of pixels. The fluxes of these sources lie in the range $0.5 \leqslant S(100) \leqslant 3\,\mathrm{Jy}$ and all of them also have 60-$\mu$m detections. Application of the correction factor $f_{\mathrm{p}\rightarrow\mathrm{t}}$, derived from the calibration observations, to the peak flux generally gave fluxes which were too low compared with the *IRAS* fluxes (after
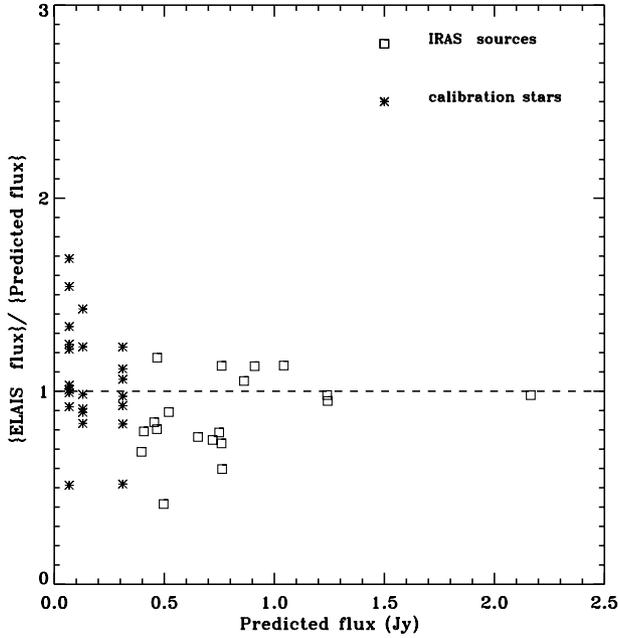
**Figure 3.** Comparison of ELAIS fluxes with *IRAS* fluxes (squares) and theoretically predicted fluxes for the calibration stars (stars). The 90-μm fluxes of the *IRAS* sources are estimated by linearly interpolating between the 60- and 100-μm fluxes. The ratio of 90- to 100-μm flux is typically 0.8. For the three calibration stars we plot all the detections (except those in the first and last pointings which make the background estimation rather difficult). The scatter in the ratio gives a measure of the reproducibility of the results. The predicted fluxes of the stars are obtained by convolving the models of Hammersley et al. (1998), for HR 6132 and 6464, and Cohen et al. (1999), for the fainter star HR 5981, with the *ISO* filter response function.

correcting for the small change in effective central wavelength of the *IRAS* and *ISO* filters) by factors of 2–3. There are a number of possible reasons for this discrepancy.

(i) First, the optical identifications of these sources appear to be galaxy pairs or galaxies with sizes comparable to or larger than the pixel size (43.5 arcsec). The *ISO* telescope PSF (for the 105-μm filter) has been approximately fitted with a Gaussian with FWHM of 50 ± 5 arcsec (Héraudeau, private communication). Clearly for such extended sources it is not appropriate to scale the peak flux by $f_{p \to t}$.

(ii) As was demonstrated by Hacking & Houck (1987) in the deep *IRAS* survey in the North Ecliptic Pole, the 100-μm fluxes of the survey proper become unreliable as the flux limit of the survey is approached (~0.5 Jy at 100 μm). The fluxes tend to be over-estimated by factors of up to 2 as they are boosted by positive noise fluctuations which are superimposed on the true source flux.

(iii) It is very unlikely that the source (even if it were point-like) would be centred in the pixel having the peak flux. In these situations $f_{p \to t}$ should be considered as a lower limit to the scalefactor.

(iv) Because of the relatively short integration time per pointing it is possible that for bright sources the signal does not reach its stabilized value, so the flux will be underestimated.

In order to determine whether a source is extended we need to know what fraction of the flux from a point source would fall in an adjacent, or diagonally placed, pixel. These fractions were estimated by Laureijs (1999) for a point source centred in a pixel.

His results show that $f_{psf}(0, 46)/f_{psf}(0, 0) = 0.06$ and $f_{psf}(46, 46)/f_{psf}(0, 0) = 0.02$ where $f_{psf}(x, y)$ is the fraction of the flux in the pixel centred at *x,y* arcsec from the point source. This assumes that all the pixels have the same roll angle. Note that although each C100 pixel is 43.5 arcsec$^2$ square, the separation of pixel centres is 46 arcsec (Klaas et al. 1994).

According to this analysis we can assume that adjacent detections with flux greater than ~15 per cent of the peak flux correspond to extended sources or members of group of sources. There are, of course, situations where this criterion will fail, that is when a point source lies at the corner or edge of a pixel. We have simulated this situation and found that we are unlikely to overestimate the flux by more than 30 per cent. Laureijs also calculated the fraction of the PSF in the whole array and found it to be ~0.8 for the C90 filter, which also sets a limit of ~30 per cent to the degree by which we would overestimate the flux of a point source in this case.

### 2.5 Summary of calibration method

In summary, our strategy for flux calibration is as follows: for sources with more than one reliable detection, the total flux is calculated by $(f_{bckg}/f_{psf}(0, 0))\sum_i F^i_{\nu,det}$, where $F^i_{\nu,det}$ are the fluxes of non-overlapping detections above 15 per cent of the peak. The factor $f_{bckg}$ is estimated to be 1.7. The factor $f_{psf}(0, 0)$ is assumed to be 0.6 (Klaas et al. 1994). For single detections we calculate the flux as $f_{bckg}F_{\nu,det}/\langle f_{psf}\rangle$, where $\langle f_{psf}\rangle$ is estimated from simulations of a point source with a FWHM of 50 arcsec at different positions in the pixel to be ~0.4.

In Fig. 3 we compare the predicted 90-μm fluxes of the *IRAS* sources with the fluxes calibrated in this way. In conclusion, our approach to the flux calibration gives fluxes that agree with those of *IRAS* sources and bright stars (which bracket the flux range covered by ELAIS) within 30–40 per cent.

## 3 RELIABILITY AND COMPLETENESS

### 3.1 Comparison to an independent pipeline

We have pursued a programme of detailed comparisons of the IC detection lists with those compiled by a pipeline developed in parallel (but somewhat later, to take advantage of a better understanding of the instrument) by the group at the Max-Planck-Institut für Astronomie (MPIA) in Heidelberg. Results from that pipeline will be described in detail by Surace et al. (in preparation). The detections obtained by the MPIA pipeline were also eyeballed with the same classification scheme applied to the IC detections.

The sample of sources on which the preliminary 90-μm counts are based is a reliable subset of the EPA list which was constructed as follows.

(i) A list of detections extracted by either pipeline and which received the top two eyeballing classifications (one or two) by at least two observers was first constructed.

(ii) The combined list was then trimmed to include only detections which received one of the top two classifications by at least three observers (275 detections).

(iii) The detections were then merged with a near-neighbour algorithm (search radius of 1 arcmin) to produce a source list consisting of 163 sources. Only one of the sources with $S > 100$ mJy was detected by the MPIA pipeline only; otherwise, the lists from the two pipelines are in complete agreement above this limit.
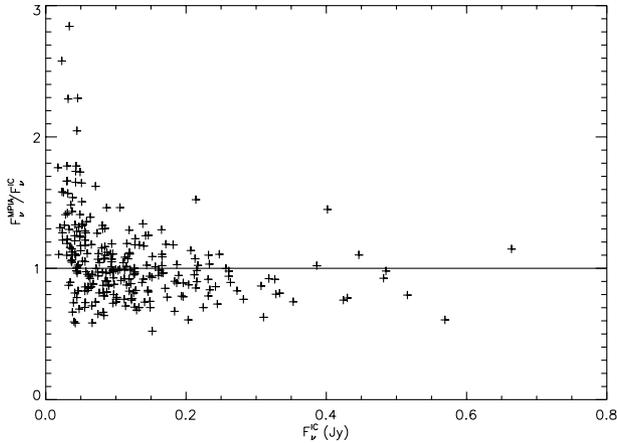
**Figure 4.** Comparison of the fluxes of the EPA reliable detections with those derived from the MPIA pipeline.

In Fig. 4 we compare the fluxes of the EPA reliable detections (*not* sources) as determined by the method described here (i.e. $f_{bckg}F_{\nu,det}$) with those derived from the MPIA pipeline. While there is considerable scatter (comparable to the scatter seen in the comparison of the backgrounds) it is rather encouraging that above 50 mJy the fluxes agree within 40 per cent. At the bright end the MPIA fluxes may be underestimated because of self-subtraction. Below 50 mJy there seems to be a group of detections where the fluxes derived by the two methods differ by factors of 2–3.

### 3.2 Simulations

The data are strongly affected by cosmic rays and other detector effects so the coverage is very inhomogeneous. In order to extract the source counts we need to quantify the incompleteness as a function of flux and position in the survey area. There are two main causes of incompleteness. First, sources that lie at the edges or corners of pixels are likely to be missed. In areas where there is redundancy (either because the overlapping mode is used or because the area has been re-observed) the probability of missing sources decreases. Secondly, some genuine sources may have been rejected at the eyeballing stage because they coincide with cosmic rays, etc.

To make a rough estimate of the degree of incompleteness due to these (and possibly other) effects we have simulated a number of rasters and processed them in an identical fashion to the survey rasters. The simulated data are constructed by adding scans of randomly placed sources on to real data extracted from several rasters (where the rasters and pixels are chosen at random). The detected sources were merged in the same way as the real sources. For practical reasons the simulated detections were eyeballed by a single observer (AE). This could introduce a bias in the completeness correction as we require confirmation (i.e. eye-balling Class 1 or 2) by at least three observers for a detection to appear in our final list of real sources. To quantify the effect of this we can use the eyeballing experience of the whole survey to find the number of detections confirmed by AE which finally appeared in the combined list (186 out of 286). For comparison, the number of detections *not* confirmed by AE which appeared in the combined list is 34. As the number of detections confirmed by AE only (286), and by at least 3 observers (186 + 34), are comparable we conclude that there is not a significant bias introduced by using
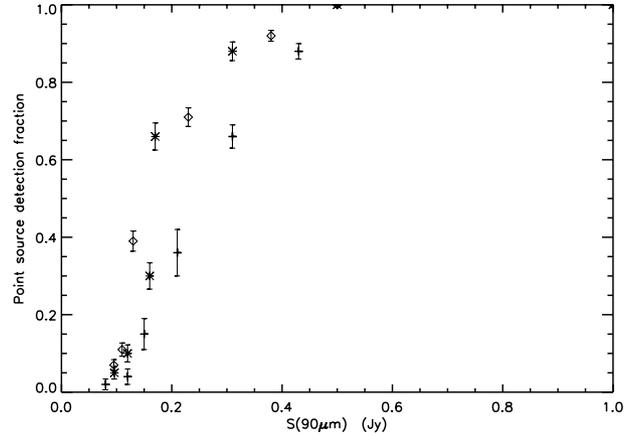


**Figure 5.** Detection fraction of point sources as a function of flux and redundancy (diamonds = 3, stars = 1, crosses = 0) estimated from simulations. The uncertainties are the statistical $\sqrt{f(1-f)N}$ errors on the detection fraction $f$, where $N$ is the number of sources in each simulation.

the eyeballing results of a single observer for the purpose of esti-mating the completeness. In order to simulate regions of multiple redundancy we simulated rasters with different steps in one of the raster dimensions. Two possibilities were simulated: half an array step, to simulate regions of single redundancy, and quarter array step, to simulate regions of triple redundancy. The sources are calibrated in the same way as the real sources.

The results of this study are plotted in Fig. 5. The fraction of sources detected increases significantly as we move from no redundancy to single redundancy. Further redundancy improves the completeness at faint fluxes.

## 4 SOURCE COUNTS

### 4.1 *IRAS* counts

We have extracted 90-μm extragalactic counts at fluxes brighter than possible with ELAIS by using the PSCz catalogue (Saunders et al. 2000). We applied a cut with galactic latitude ($|b| > 20$) which limits the areal coverage to 7.642 sr (Rowan-Robinson et al. 1991) and the number of galaxies to 11 405. We also excluded galaxies with low *IRAS* flags ($fqual < 3$) at 100 μm. The resulting sample consists of 8529 galaxies. The 90-μm flux of each galaxy is estimated by linearly interpolating between the 60- and 100-μm fluxes (by design all galaxies in the PSCz catalogue have reliable 60-μm fluxes).

The *IRAS* counts are plotted in Fig. 7 (see later). The structure in the counts above 5 Jy, which is also evident in the 60-μm counts (Hacking, Condon & Houck 1987), is probably caused by a local excess in the source density dominated by the Virgo cluster.

The PSCz catalogue only includes galaxies with $S(60) > 0.6$ Jy. *IRAS* galaxies are known to have $S(100)/S(60)$ ratios at least as high as 3.5 (e.g. Rowan-Robinson & Crawford 1989; Efstathiou et al., in preparation). A 90-μm sample drawn from PSCz is therefore bound to be incomplete below 2 Jy. This incompleteness is most probably the reason for the flattening of the *IRAS* counts between 1 and 2 Jy.

### 4.2 ELAIS counts

To extract the source counts we need to determine the area over which the survey is sensitive to as a function of flux. To do that we

use the results from the simulations given in Fig. 5. While we have not simulated sources with $S > 0.5$ Jy we can reasonably assume that we are close to 100 per cent complete for those fluxes as we have detected all *IRAS* sources in the fields. We only consider regions of redundancy three or less in this paper (amounting to a total of 11 deg$^2$) and therefore exclude the S2 area. All of the small areas of special scientific interest are also excluded as some are centred on known objects. The resulting areal coverage as a function of flux is given in Fig. 6. The counts are corrected for incompleteness by normalizing each source by the area over which each source could be found (Hacking & Houck 1987; Oliver et al. 1997). The resulting integral counts are given in Fig. 7. Flux uncertainties of $\pm 0.15$ dex are also indicated. The uncertainties in the number counts are the Poisson errors, uncertainties in the effective area have not been included.

The sources presented here are extracted from a reliable subset of the EPA sources as described in Section 3. About 42 per cent of the sources brighter than 140 mJy are detected in at least two neighbouring or overlapping pixels. About 67 per cent of the sources also have an association with a mid-infrared ELAIS source within a 1-arcmin radius.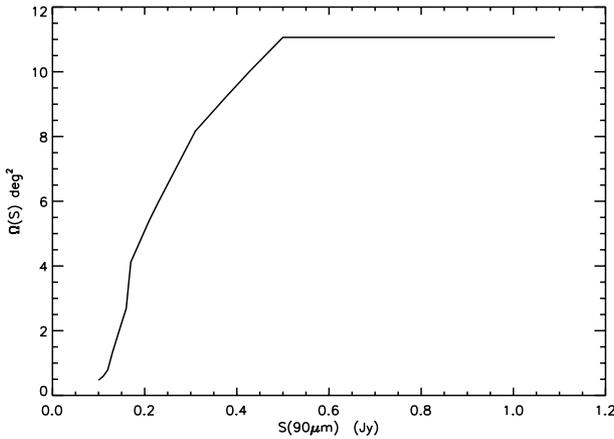 Given the relatively low source density of ELAIS sources the probability of a chance association is only a few per cent. We also note that there are good optical identifications associated with the majority of the PHOT sources.

To obtain an estimate of the likely contamination of our sample by cirrus we use the models of Gautier et al. (1992). Our observing mode is different from either of the two cases considered in that paper as our reference (background) position is offset by $67-390$ arcsec. If we use their double-aperture mode with this range of offset and assume the slope of the power spectrum of the cirrus is in the range $-2.6$ to $-3.8$, then the expected rms cirrus confusion noise is predicted to be in the range $0.2-3.1$ mJy for a background intensity of 1 MJy sr$^{-1}$. The latter is about a factor of 2 brighter than that found in the typical ELAIS area (Paper I), so it is very unlikely that any of our sources are caused by cirrus.

We estimate the slope of the counts (assuming they can be described by a power law) by applying a $\chi^2$-minimization procedure (the IDL routine linfit) on the model

$$\log_{10}\left(\frac{dN}{d\log_{10} S}\right) = a + b\log_{10} S.$$

In the range $0.158-1$ Jy we find $a = 3.71 \pm 0.13$ and $b = -1.92 \pm 0.23$. If we use only sources found in areas with redundancy in our analysis, the estimated parameters are $a = 3.65 \pm 0.22$ and $b = -2.11 \pm 0.34$. We also estimate the slope of the *IRAS* counts in the range $2-20$ Jy (where the effects of incompleteness and large-scale structure are minimized) to be $a = 3.73 \pm 0.02$ and $b = -1.48 \pm 0.03$. The ELAIS counts therefore show some evidence for departure from the Euclidian slope. However, because of the limited statistics of the ELAIS survey and the incompleteness of *IRAS* at around 1 Jy it is difficult to constrain from this study the flux at which this takes place.

## 5 DISCUSSION

### 5.1 Comparison with evolutionary models

The recent dramatic improvement in observational constraints in the star-formation history of the Universe and therefore the evolution of the starburst galaxy populations in the optical/UV, and recently the submillimetre, has stimulated the development of



**Figure 6.** Area (in deg$^2$) over which the sensitivity of the survey is $S$. The area is estimated from simulations for different values of $S$ and different degrees of redundancy.
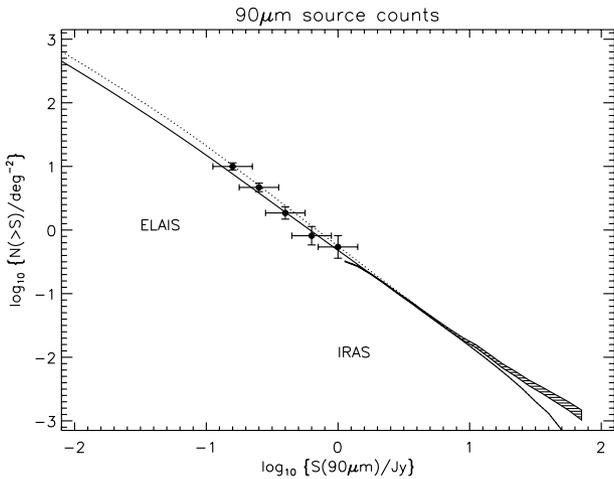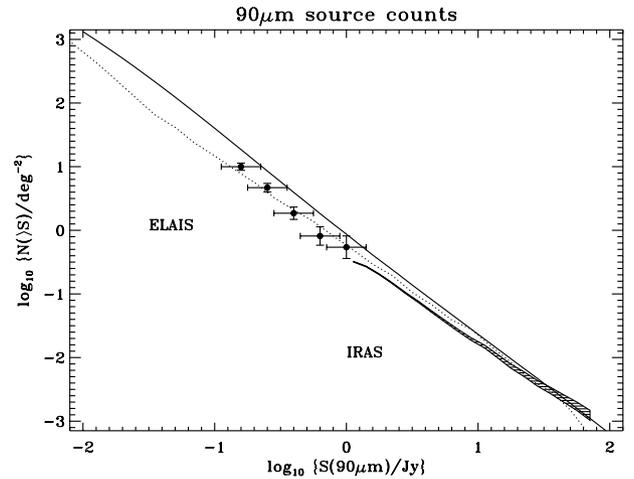


**Figure 7.** ELAIS/IRAS 90-μm source counts. The solid and dotted lines are the counts predicted by the models A and E (respectively) of Guiderdoni et al. (1998).



**Figure 8.** ELAIS/IRAS 90-μm source counts. The solid line gives the counts predicted by the model of Rowan-Robinson (1999). The dotted line shows the counts predicted by the model of Franceschini.

evolutionary models (Pei & Fall 1995; Pearson & Rowan-Robinson 1996; Franceschini et al. 1997; Guiderdoni et al. 1998; Rowan-Robinson 1999). In Figs 7 and 8 we compare the observed counts with the models of Rowan-Robinson, Guiderdoni et al. and Franceschini et al.. The counts predicted by the models differ by a factor of 3–4 at about 100 mJy and the ELAIS counts can potentially discriminate between them.

The model of Guiderdoni et al. is set within the framework of hierarchical growth of structures according to the cold dark matter model, and extends earlier studies (e.g. by Cole et al. 1994) to the IR/submillimetre wavelength regime. In Fig. 7 we plot the prediction from their models A and E. The latter model incorporates a heavily extinguished (ULIRG) population, assumed to dominate at high redshift in order to account for the far-IR background.

The starting point in the model of Rowan-Robinson (1999) is an assumed star formation history of the Universe, described by an analytic formula involving two free parameters ($P, Q$). The star formation rate is assumed to evolve as a result of pure luminosity evolution. The parameters $P$ and $Q$ are then constrained by fits to the observed star formation history, the observed 60–175 and 850-$\mu$m counts and the observed far-IR background. The model assumes a number of IR galaxy populations which are modelled with the radiative transfer models of Efstathiou, Rowan-Robinson & Siebenmorgen (2000). The prediction of the Rowan-Robinson model is compared with the observed counts in Fig. 8.

The model of Franceschini et al. (in preparation) assumes that the extragalactic population is composed of two components with different evolution properties: (1) a non-evolving galaxy population in which the far-IR flux is mostly contributed by evolved stars; (2) a population of strongly evolving starbursts, with peak emissivity around redshift 0.8 and roughly constant emissivity at higher $z$. The evolution rate for population (2) is optimized to reproduce the mid-IR counts and redshift distributions. The model of Franceschini is also plotted on Fig. 8.

While the observed counts tentatively favour the Guiderdoni model, the uncertainties due to flux calibration and correction for incompleteness do not allow us to definitely discriminate between the models at the present stage. A more detailed analysis of the ELAIS 90-$\mu$m survey (already under way) should be able to discriminate between the models. Further discrimination of the two models should be possible with the redshift distributions of the detected galaxies. The models of Franceschini et al. and Rowan-Robinson predict that the vast majority of sources at $S > 100$ mJy will be at redshifts less than 1. The Guiderdoni et al. model overpredicts the number of high redshift galaxies in the North Ecliptic Pole (NEP) survey, although the counts in the latter are known to be dominated by a supercluster (Ashby et al. 1996). The ELAIS survey was specifically designed (Paper I) to minimize the effects of large-scale structure.

### 5.2  Comparison with other infrared and submillimetre surveys

Until recently the deep IRAS 60 $\mu$m survey (Hacking & Houck 1987) provided the deepest extragalactic source counts in the infrared. Augmented with counts from shallower surveys (e.g. Rowan-Robinson et al. 1991) they provided the basis for studies of the evolution of the starburst galaxy population (Hacking et al. 1987; Oliver, Rowan-Robinson & Saunders 1992; Oliver et al. 1995; Pearson & Rowan-Robinson 1996). Unfortunately redshift measurements of the redshift sources, which should have been able to constrain further the form of evolution, discovered the presence of a $z = 0.088$ supercluster in the NEP field (Ashby et al. 1996).

Oliver et al. (1997) confirmed the strong evolution seen in *IRAS* surveys with deep counts at 6.7 and 15 $\mu$m in the Hubble deep field. Counts at 15 $\mu$m well in excess of no-evolution expectations were also reported by Elbaz et al. (1999). Serjeant et al. (2000; Paper II) found the evolving high-$z$ population dominates over the local counts at $S(15) < 10$ mJy.

With the advent of SCUBA, submillimetre surveys (at 850 $\mu$m) which exploited the negative $K$-correction arising from the spectral shape of starburst galaxies, detected source densities two to three orders of magnitude higher than expected from non-evolving models (Smail et al. 1997; Barger et al. 1998; Hughes et al. 1998; Eales et al. 1999). While the process of identifying and determining the properties of these SCUBA sources is still incomplete, it appears that a number of them are similar to ULIRGs at $z \sim 2$–4. SCUBA surveys appear to have resolved 94 per cent and 34 per cent of the *COBE*–FIRAS background values at 850 and 450 $\mu$m, respectively (Blain et al. 1999).

FIRBACK 175-$\mu$m counts in the Marano 1 field also appear to have shown an upturn in the counts (Puget et al. 1999). These counts are 3 times higher than the models of Guiderdoni et al. and Franceschini et al. However, 175-$\mu$m counts in a larger area (Dole et al. 1999) suggest that the counts in the Marano field may have been anomalously high. It is also not clear whether the excess in the counts, if any, is caused by high-redshift starbursts or local cold galaxies. Counts 3–10 times higher than expected from no-evolution models were also found by Kawara et al. (1998) in their 175-$\mu$m survey of the Lockman Hole. More results are expected from FIRBACK and ELAIS surveys at this wavelength. Brighter counts are also expected from the *ISO* Serendipity survey (Bogun et al. 1996; Stickel et al. 1998).

The extensive multiwavelength coverage and follow-up programme of ELAIS ensures that, unlike other far-IR surveys where resolution and sensitivity can be a serious obstacle, the 90-$\mu$m galaxies will be thoroughly studied (e.g. Morel et al. in preparation) and will therefore provide a firm basis for studying the evolution of dust-enshrouded galaxies.

A more detailed analysis of the ELAIS PHOT survey is underway and results will be presented in subsequent papers in this series.

### 6  CONCLUSIONS

We have presented 90-$\mu$m source counts extracted from the catalogue produced by the ELAIS preliminary analysis and PSCz redshift survey. All but one of the sources brighter than 100 mJy have been confirmed by an independent pipeline developed at MPIA, Heidelberg. We compare our estimated fluxes with *IRAS* fluxes and models for standard stars and estimate the uncertainty in flux calibration to be about 30–40 per cent.

The ELAIS counts extend the *IRAS* counts by an order of magnitude in flux. The slope of the counts in the 0.158–1 Jy range shows some evidence for departure from the Euclidian slope. This is consistent with the strong evolution seen in other infrared and submillimetre surveys.

Within the uncertainties associated with the flux calibration of the survey, the counts agree with the strongly evolving models of Rowan-Robinson (1999), Guiderdoni et al. (1998) and Franceschini et al. We expect the redshift distributions arising from the spectroscopic follow-up of the survey to allow us to discriminate between these models.

## ACKNOWLEDGMENTS

## REFERENCES

Ashby M. L. N., Hacking P. B., Houck J. R., Soifer B. T., Weisstein E. W., 1996, ApJ, 456, 428
Barger A. J., Cowie L. L., Sanders D. B., Fulton E., Taniguchi Y., Sato Y., Kawara K., Okuda H., 1998, Nat, 394, 248
Blain A., Ivison R., Kneib J.-P., Smail I., 1999, astro-ph/9908024
Bogun S. et al., 1996, A&A, 315, L71
Cohen M. et al., 1999, AJ, 117, 1864
Condon J. J., Huang Z.-P., Yin Q. F., Thuan T. X., 1991, ApJ, 378, 65
Dole H. et al., 1999, in Cox P., Kessler M. F., eds, The Universe as seen by ISO. ESA-SP 427, p. 1031
Eales S. et al., 1999, ApJ, 515, 518
Efstathiou A., Rowan-Robinson M., 1995, MNRAS, 273, 649
Efstathiou A., Rowan-Robinson M., Siebenmorgen R., 2000, MNRAS, 313, 734
Elbaz D. et al., 1999, A&A, 351, L37
Fixsen D. J., Dwek E., Mather J. C., Bennett C. L., Shafer R. A., 1998, ApJ, 508, 123
Franceschini A., Mazzei P., De Zotti G., Danese L., 1994, ApJ, 427, 140
Gabriel C. et al., 1997, in Hunt G., Payne H. E., eds, ASP Conf. Ser. Vol. 125, Proc. ADASS VI Conf. Astron. Soc. Pac., San Francisco, p. 108
Gautier T. N., Boulanger F., Perault M., Puget J. L., 1992, AJ, 103, 1313
Granato G. L., Danese L., 1994, MNRAS, 268, 235
Guiderdoni B., Hivon E., Bouchet F. R., Maffei B., 1998, MNRAS, 295, 877
Hacking P., Houck J. R., 1987, ApJS, 63, 311
Hacking P., Condon J. J., Houck J. R., 1987, ApJ, 316, L15
Hammersley P., Jourdain de Muizon M., Kessler M. F., Bouchet P., Joseph R. D., Habing J., Salama A., Metcalfe L., 1998, A&AS, 128, 207
Hauser M. G., Gillett F. C., Low F. J., Gautier T. N., Beichman C. A., Aumann H. H., Neugebauer G., Baud B., Boggess N., Emerson J. P., 1984, ApJ, 278, 15
Hauser M. G. et al., 1998, ApJ, 508, 25
Hughes D. et al., 1998, Nat, 394, 241
Kessler M. et al., 1996, A&A, 315, 27
Kawara K. et al., 1998, A&A, 336, L9
Klaas U., 1994, ISOPHOT observer's manual, Version 3.1
Krügel E., Siebenmorgen R., Zota V., Chini R., 1998, A&A, 331, L9
Lagache G., Abergel A., Boulanger F., Puget J.-L., 1998, A&A, 333, 709
Laureijs R., 1999, http://www.iso.vilspa.esa.es/users/expl_lib/PHT_list
Lemke D. et al., 1996, A&A, 315, 64
Madau P., Ferguson H. C., Dickinson M. E., Giavalisco M., Steidel C. C., Fruchter A., 1996, MNRAS, 283, 1388
Oliver S., Rowan-Robinson M., Saunders W., 1992, MNRAS, 256, 15P
Oliver S. J. et al., 1995, in Maddox S. J., Aragon-Salamanca A., eds, Wide field spectroscopy and the distant universe. World Scientific, Singapore, p. 274
Oliver S. et al., 1997, MNRAS, 289, 471
Oliver S. J. et al., 2000, MNRAS, 316, 749 (Paper I)
Pearson C., Rowan-Robinson M., 1996, MNRAS, 283, 174
Pei Y. C., Fall S. M., 1995, ApJ, 454, 69
Pier E., Krolik J., 1992, ApJ, 399, L23
Puget J.-L., Abergel A., Bernard J.-P., Boulanger F., Burton W. B., Desert D.-X., Hartmann D., 1996, A&A, 308, L5
Puget J.-L. et al., 1999, A&A, 345, 29
Reach W. T. et al., 1996, A&A, 315, L381
Rowan-Robinson M., Crawford J., 1989, MNRAS, 238, 523
Rowan-Robinson M., Saunders W., Lawrence A., Leech K., 1991, MNRAS, 253, 485
Rowan-Robinson M., 1999, astro-ph/9906308
Rowan-Robinson M., Efstathiou A., 1993, MNRAS, 263, 675
Saunders W. et al., 2000, MNRAS, 317, 55
Schlegel D., Finkbeiner D., Davis M., 1998, ApJ, 500, 525
Schulz B. et al., 1999, http://www.iso.vilspa.esa.es/users/expl_lib/PHT_list
Serjeant S. et al., 2000, MNRAS, 316, 768 (Paper II)
Smail I., Ivison R. J., Blain A. W., 1997, ApJ, 490, L5
Steidel C. C., Giavalisco M., Pettini M., Dickinson M., Adelberger K. L., 1996, ApJ, 462, L17
Stickel M. et al., 1998, A&A, 336, 116

This paper has been typeset from a TEX/LATEX file prepared by the author.